Journal of Materials Chemistry A

Accepted Manuscript

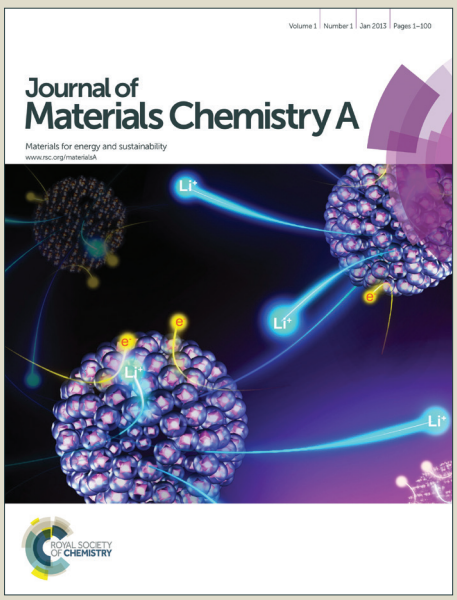

ROYAL SOCIETY OF CHEMISTRY

www.rsc.org/materialsA

Cite this: DOI: 10.1039/c0xx00000x

www.rsc.org/xxxxxx

ARTICLE TYPE

Synthesis of $MoS_2/SrTiO_3$ composite materials for enhanced photocatalytic activity under UV irradiation

Jiahui Liu,† Li Zhang,† Naixu Li, Qingwen Tian, Jiancheng Zhou,* and Yueming Sun

Received (in XXX, XXX) Xth XXXXXXXXX 20XX, Accepted Xth XXXXXXXXX 20XX

DOI: 10.1039/b000000x

A novel composite material $MoS_2/SrTiO_3$ has been successfully prepared via a two-step simple hydrothermal method. The photocatalytic performance of $MoS_2/SrTiO_3$ composites for degradation of MO organic dyes under UV light irradiation and the effect of loading amount of MoS_2 were investigated. For the first time, it was found that the as-prepared composites show high degradation rate and the photocatalytic activity over pure $SrTiO_3$ can be significantly enhanced by loading MoS_2. Importantly, there is an optimal loading amount MoS_2 on the $SrTiO_3$ in terms of degradation rate. In addition, the composite materials $MoS_2/SrTiO_3$ with 0.05 wt % of MoS_2 show the best photocatalytic activity with the degradation rate as high as 99.81% after 60 min irradiation time. The promoting effect caused by MoS_2 can be due to suppressing recombination between electrons and holes. This study demonstrates a high potential of the developing of environmentally friendly, cheap non-noble metal composite materials for photocatalytic degradation.

1 Introduction

In recent years, wastewater from textiles, paint, printing, cosmetics and other industries has become one of the most concerning environmental problems because the wastewater containing various kinds of organic dyes impart adverse effects on people's life and ecosystem[1-5]. Due to the stability of synthetic dyes and the high salinity of wastewater with dyes, this kind of wastewater is more difficult to treat. Conventional methods used in wastewater treatment such as adsorption, combined coagulation and flocculation, biodegradation and activated sludge can not fully meet the requirements for this type wastewater. In addition, these methods transfer the organic dyes pollutants from liquid phase to other media resulting in secondary pollution [6]. As a consequence, to prevent environmental contamination, it is an imperative task to develop environmentally friendly technologies for the degradation of synthetic organic dyes which are resistant to conventional methods and not easily removed in water treatment plant [7]. Recently, semiconductor photocatalysis has proved to be efficient in the advanced oxide process which refers to chemical treatment to remove pollutant from wastewater through oxidation [8-10]. And photocatalysis has emerged as one of the most promising technologies. Moreover, a wide range of organic dyes can be oxidized quickly and non-selectively [11-16].

Perovskite type oxides with ABO_3 structure (A is a rare earth metal with a large ionic radius; B is a transition metal with a small ionic radius) are one class of promising photocatalysis materials[17]. Due to their multifunctional and exotic properties, they can be applied to gas, solid and liquid phase reactions [18]. As a promising photocatalyst, strontium titanate ($SrTiO_3$) has sparked a growing interest because of its outstanding physicochemical properties such as having larger number of photocatalytic sites, its excellent photo corrosion resistibility, thermal stability and good structure stability as a host for metal loading [19]. These properties make $SrTiO_3$ capable for splitting water into H_2 and O_2, degradation of organic pollutants and other photo conversion reactions under ultraviolet light irradiation.

In general, photocatalytic process can be summarized as follows: firstly, photoexcited electrons were induced from the valence band to the conduction band, leaving equivalent vacant sites in the valence band and thus electron and hole pair is generated; then photoexcited electrons and holes migrate to the surface; finally, photoexcited electrons and holes react with electron donors and electron acceptors at the surface of semiconductor photocatalyst, repectively [20-22]. In the second step, a high recombination ratio between electron and hole occurs, which leads to input light energy dissipating. In order to prevent the recombination of electron and hole pairs, many researchers [23-24]have tried to dope or incorporate a small amount of noble metals, transition metals oxide, non-metal and other elements on the semiconductor surface, which can further enhance its photocatalytic performance.

Many attempts have been made to synthesis composites photocatalyst to facilitate charge rectification and improve carrier separation [25]. In such photocatalyst, the materials loaded on semiconductor photocatalyst play an essential role in improving the photocatalytic activity and synergetic effects on carrier separation and photocatalytic efficiency have been studied in recent years. Therefore, to enhance the activities of photocatalyst, it is extraordinarily important to load a suitable material [26-27]. As a novel semiconductor featuring a layered structure, molybdenum

disulfide (MoS_2) which is composed of Mo atoms sandwiched between two layers of sulfur atoms shows remarkable effects in water splitting and degradation of pollutants when coupled with other semiconductors such as TiO_2, CdS, g-C_3N_4 and graphene oxide[28-35]. J. G. Yu et al.[33] synthesized a new composite material consisting of TiO_2 nanocrystals grown in the presence of a layered MoS_2/graphene hybrid as a high-performance photocatalyst for H_2 evolution. C. Li et al.[35] loaded MoS_2, a substitute for the noble metals, as a cocatalyst on CdS, which exhibited enhanced photocatalytic activity for the H_2 production from a lactic acid solution under visible light. However, there have been few reports about $SrTiO_3$ coupled with MoS_2 [36-37]. However, two foreign elements were doped with $SrTiO_3$ in these literatures and the synthesis method was complicated. In addition, the synthesized materials were not applied to wastewater treatment.

Herein, we report the fabrication of novel composites, i.e. few layer MoS_2, a cheap non-noble metal, loaded on $SrTiO_3$ using a two-step simple hydrothermal method and their photocatalytic performances in the degradation of methyl orange (MO) under UV light irradiation were investigated. In addition, the effect of MoS_2 content on photocatalytic activity was also evaluated. To the best our knowledge, there are no reports concerning the degradation of MO with this kind of $MoS_2/SrTiO_3$ composite materials. As a proof of concept, we demonstrate that the synthesized $MoS_2/SrTiO_3$ composites are an excellent photocatalyst for the degradation of MO.

2 Experimental methods

2.1 Chemicals

Citric acid monohydrate, tetraisopropyl orthotitanate, strontium nitrate ($Sr(NO_3)_2$), sodium hydroxide (NaOH), sodium molybdate (Na_2MoO_4), thioacetamide (CH_3CSNH_2), methyl orange (MO), anhydrous ethanol, acetic acid. Deionized water was used throughout the whole experiment. All of the chemicals were purchased from the Shanghai Chemical Reagent Company in analytical grade, and were used as received without further purification.

2.2 Procedure for the synthesis of the $MoS_2/SrTiO_3$ composite materials

2.2.1 Synthesis of $SrTiO_3$

$SrTiO_3$ was synthesized according to the method reported by J. H. Ye et al.[38] with some modification. Briefly, citric acid monohydrate (0.060 mol) was dissolved in ethanol (15 mL) and tetraisopropyl orthotitanate (0.005 mol) was subsequently added. The mixture was mechanically stirred for 10min and then aqueous solution containing $Sr(NO_3)_2$ (0.005 mol) and NaOH (0.05 mol) were successively added drop by drop under ultrasonic dispersion with mechanical stirring at room temperature for 20 min. Afterwards, the resulting solution was sealed in a Teflon-lined stainless-steel autoclave. The autoclave was heated to 150℃ and maintained at that temperature for 36 h. The autoclave was then allowed to cool to room temperature naturally. After centrifugation, the product was washed with deionized water, acetic acid and ethanol several times. Finally, the obtained product was vacuum dried at 60℃ for 12 h for future use.

2.2.2 Synthesis of MoS_2

MoS_2 was successfully prepared according to a simple hydrothermal method. In general, Na_2MoO_4 (0.05mol) and CH_3CSNH_2 (0.25mol) were dissolved into distilled water (20mL) and ethanol (20mL). Then the following step for the mixture was accompanied by ultrasonic and magnetic stirring, respectively. The mixed solution was transferred to a Teflon-lined stainless-steel autoclave, which was subsequently heated to 200℃ for 48h. Then the product was obtained by centrifuge after the solution was taken from the cool autoclave. Subsequently, the product was washed with ethanol several times. The product was then vacuum dried at 60℃ for 12 h for next research.

2.2.2 Fabrication of $MoS_2/SrTiO_3$ composites

$SrTiO_3$ particles coupled with x wt % MoS_2 ($0 \le x \le 5$) were prepared through a hydrothermal reaction as follows: the starting materials, $SrTiO_3$, Na_2MoO_4, and CH_3CSNH_2, were added to a breaker in a $SrTiO_3$: Na_2MoO_4: CH_3CSNH_2 molar ratio of 87.25: x: 5x, then mixed with deionized water (20 mL) and ethanol (20 mL) under vigorous mechanical stirring for 30 min after ultrasonic dispersion for 20 min. Afterwards, the mixture were sealed in PPL-lined stainless-steel autoclave. The autoclave was heated to 200℃ for 48 h. Then the autoclave was allowed to cool to room temperature naturally. The mixture was centrifuge to obtain the synthesized product. The product was washed with deionized water and ethanol several times. The final product was vacuum dried at 60℃ for 12 h. The composite materials were hereafter referred to as $MoS_2/SrTiO_3$.

2.3 Photocatalytic activity testing

The photocatalytic performances of the as-prepared $MoS_2/SrTiO_3$ were evaluated through the photocatalytic degradation of MO in aqueous solution under UV light irradiation (GGZ 100-1, 100W, with a maximum emission wavelength of 365 nm) at room temperature. Typically, a quantity of 7.5 mg of MO was dissolved in 250 mL deionized water to yield a MO concentration of 30 mg L^{-1}. Then 0.30g of $MoS_2/SrTiO_3$ photocatalyst was dispersed in 30 mg L^{-1} aqueous MO dye solution. The suspensions were continuous magnetically stirred in the dark for 30 min to reach the adsorption-desorption equilibrium. The first sample was extracted before UV light irradiation. Under ambient conditions and stirring, the suspensions were exposed to UV light irradiation. 5 mL of the sample was periodically extracted after every 15 min and then centrifuged to remove the photocatalyst from the solution. Finally, the absorbance of filtrates was measured by a spectrophotometric technique. The photocatalytic performance was measured by oil removal rate, which is calculated from the equation:

$$D = \frac{C_0 - C}{C_0} \times 100\%$$

where D (%) is the degradation rate, C_0 (mg L^{-1}) denotes the initial MO dye concentration, C (mg L^{-1}) represents the MO dye concentration in filtrates after irradiation.

2.4 Characterization

The morphology of the samples was characterized by transmission electron microscopy (TEM) with a Hitachi H-600microscope operating at 120 kV. Scanning electron

microscopy (SEM) was performed to analyse the morphology by using JSM-6700F. X-ray photoelectron spectroscopy (XPS) measurements were performed on a 2000 XPS system with a monochromatic Al K_α source and a charge neutralizer. X-ray diffraction (XRD) patterns were recorded using a Rigaku D/MAX-R diffractometer with a copper target at 40 kV and 30 mA. The power samples were spread on a sample holder and the diffraction grams were recorded from 5-90 ° at the speed of 5 ° min^{-1}. UV-vis absorption spectra were measured with a Shimadzu UV 3600 spectrometer. The spectra were recorded from 300 to 600 nm. And diffuse reflectance spectroscopy was also carried out using a Shimadzu UV 3600 spectrometer with the wavelength from 200 to 800 nm.

3 Results and discussion

In order to investigate the crystal structures of the as-prepared $SrTiO_3$, $MoS_2/SrTiO_3$ composites, XRD experiments were carried out. The XRD patterns of the samples are shown in Fig. 1. For the pure $SrTiO_3$ sample (curve b in Figure 1), it possesses the dominant diffraction peaks at 2θ angel are 32.4 °, 39.9 °, 46.5 °, 57.7 °, 67.6 °, and 77.1 °, representing the indices of (110), (111), (200), (211), (220), and (310) lattice planes, respectively. The diffraction peaks match the standard peaks of $SrTiO_3$ (JCPDS card No. 35-0734), which reveals that $SrTiO_3$ samples were successfully synthesized and the synthesized $SrTiO_3$ is a cubic perovskite structure. As for the pure MoS_2 sample (curve a in Figure 1), it can be noted that the detected three main diffraction peaks, i.e., 17.4 °, 34.2 °, and 56.7 ° can be assigned to the (002), (100), and (110) lattice planes in the hexagonal phase MoS_2 (JCPS card No. 37-1492). As shown in curve c and d, no typical diffraction peaks of MoS_2 are not observed in the diffraction peaks patterns of $MoS_2/SrTiO_3$ composites, which may be due to the low content of MoS_2. The diffraction peaks of $MoS_2/SrTiO_3$ composites are similar to those of pure $SrTiO_3$, indicating that the presence of MoS_2 does not lead to the new formation of secondary phase in the samples.

The surface morphologies of the prepared samples were analysed by SEM and TEM. As revealed in Fig. 2a and 2b, the pure MoS_2 prepared by hydrothermal method possess a flower-like structure, which is composed of MoS_2 nanosheets. Compared with Fig. 3a, the image of Fig. 3d reveals that $MoS_2/SrTiO_3$ nanoparticles, a mean diameter of about 30 nm, were assembled to form spherical spheres $MoS_2/SrTiO_3$ composites and the incorporation of MoS_2 can not significantly change the morphology of $SrTiO_3$. According to the energy-dispersive X-ray spectrometry (EDS) in Fig. 3c, the existence of Mo and S element in the $MoS_2/SrTiO_3$ composites has been proved. Moreover, from Fig. 3e and 3f, clear lattice fringe of 0.62nm corresponded to the 002 plane of MoS_2 can be observed. Therefore, it is clearly that MoS_2 can be successfully loaded on the surface of $SrTiO_3$.

X-ray photoelectron spectroscopy (XPS) was used to analysis the binding states of the elements on the surface of $MoS_2/SrTiO_3$ composites. In Fig. 4b, the high-resolution XPS spectra of $MoS_2/SrTiO_3$ show that the binding energies of Mo $3d_{3/2}$ and Mo $3d_{5/2}$ peaks are located at 232.3 and 229.1 eV, respectively, suggesting that Mo^{4+} existed in the sample. The values are similar to previously report for MoS_2 [28,34]. In addition, from Fig. 4c, it can be seen that the spectra of $MoS_2/SrTiO_3$ in the S 2p region show that binding energy at 163.2 eV for S $2p_{1/2}$ and 162.5 eV for S $2p_{2/3}$, respectively, which can be assigned to S^{2-}. Clearly, a higher binding energy of Sr 3d of $MoS_2/SrTiO_3$ shift about 0.33 eV can be observed in Fig. 4d. Moreover, similar shift can also be observed in the XPS spectra of Ti 2p and O 1s. The phenomenon can be occurred because the electrons can transfer from $SrTiO_3$ to MoS_2 [34].

To investigate optical absorption properties of the samples, diffuse reflectance spectroscopy (DRS) was carried out. Fig. 5 shows absorption spectra of MoS_2, $SrTiO_3$ and $MoS_2/SrTiO_3$ composites, which are transformed from their corresponding diffuse reflectance spectra according to the Kubelka–Munk (K–M) theory. For the pure $SrTiO_3$, the significant steep absorption edge located at about 392 nm can be assigned to its intrinsic band gap absorption. The band gap energy of $SrTiO_3$, which can be determined based on the equation E (eV) =1240/λ (nm), is calculated to be 3.2 eV. The value is identical to that of $SrTiO_3$ in many reports [39-40]. The pure synthesized MoS_2 in this work shows absorption at 715 nm, while bulk MoS_2 has an absorption edge at 1040 nm (band gap of 1.23 eV) [41]. This large blue-shift can be attributed to the strong quantum confinement effect of the thin MoS_2 sheet. Noticeably, the absorption band of the synthesized $MoS_2/SrTiO_3$ composites was mainly in the UV light range. After loading a certain amount of MoS_2, the slightly enhanced absorption, compared with pure $SrTiO_3$, can be observed.

The photocatalytic activity of the $MoS_2/SrTiO_3$ composites was evaluated by degrading the organic dye MO. Fig. 6 shows the degradation rate of MoS_2, $SrTiO_3$ and $MoS_2/SrTiO_3$ composites with 0.01, 0.05, 0.1, 0.5, 1, 3 and 5 wt % loading amount of MoS_2 for the degradation of MO. It can be observed that the photocatalytic degradation activity of pure $SrTiO_3$ is not good. However, the photocatalytic degradation activity of $MoS_2/SrTiO_3$ composites increases. It is worthy to note that the photocatalytic activity is significantly enhanced by the loading MoS_2 to some extent. Obviously, there is an optimal loading amount MoS_2 on the $SrTiO_3$ in terms of degradation rate. When the loading of MoS_2 was 0.05 wt %, the photocatalytic activity of $MoS_2/SrTiO_3$ composites is best with the degradation rate as high as 99.81% after 60 min irradiation time. The photocatalytic performance of 0.05 wt % is more excellent than those from the $MoS_2/SrTiO_3$ composites with lower and higher loading of MoS_2. Even the degradation rate of $MoS_2/SrTiO_3$ composites (3 and 5 wt % of MoS_2) is worse than the pure $SrTiO_3$.

Therefore, the $MoS_2/SrTiO_3$ composites play an important role in improving the photocatalytic activity when the loading amount of MoS_2 is appropriate. It can be ascribed to the efficient charge separation of $SrTiO_3$ by MoS_2 to suppress the electron-hole recombination, which greatly enhances the degradation rate. With the loading of MoS_2 increasing from 0.05 to 5 wt %, a large quantity of black MoS_2 can give rise to shielding of the active sites and also decrease the intensity of UV light irradiation through the depth of reaction aqueous solution. As a consequence, excessive loading of MoS_2 results in the unsatisfactory photocatalytic performance of $MoS_2/SrTiO_3$ composites.

The UV-vis absorption spectra of MO at 30 min irradiation time by pure $SrTiO_3$ and $MoS_2/SrTiO_3$ composites (0.01, 0.05, 0.1, 0.5, 1, 3 and 5 wt % loading of MoS_2) were shown in Fig. 7.

Because the intensity of peak is relevant to the concentration of MO, it can be used to evaluate the MO degradation performance. As can be noted, the intensity of the maximum absorption peak at 460 nm is weakest when the loading of MoS_2 is 0.05 wt %. In addition, the peak becomes weak with the increase in the loading of MoS_2 from 5 to 0.05 wt %. The results accord with the changes of degradation rate. Fig. 8a displays changes in UV-vis absorption spectra of MO aqueous solution at the varied irradiation time using $MoS_2/SrTiO_3$ composites (0.05 wt % of MoS_2) under UV light irradiation. Clearly, the intensity of absorption peak gradually declines with increasing its irradiation time during the photocatalysis process, which represents the concentration of MO decreases by degrees. It is observed that $MoS_2/SrTiO_3$ composites (0.05 wt % of MoS_2) shows nearly complete degradation of MO in 60 min. Moreover, the intensity of absorption peak was almost the same when irradiation time was 50 min and 60 min. So it is difficult to observe the curve of absorption spectra at 50 min. As revealed in Fig. 8b, the colour of MO dyes solutions becomes transparent step by step with the increase in the irradiation time. And the first sample under dark for 0.5 h has no change in colour of MO dyes solutions, which indicates that $MoS_2/SrTiO_3$ composites and UV light irradiation are essential to MO dyes degradation.

A mechanism proposed for the high photocatalytic activity of the $MoS_2/SrTiO_3$ composites is illustrated in Fig. 9. Because the conduction band position of $SrTiO_3$ is higher than that of MoS_2, the electrons can easily transfer from $SrTiO_3$ to MoS_2. Under UV light irradiation, the photo-excited electrons VB of $SrTiO_3$ are directly transferred to CB of $SrTiO_3$, creating holes in the VB [42]. The photo-generated electrons and holes are inclined to recombine quickly without MoS_2 loading, causing the low photocatalytic activity. However, after introducing MoS_2, electrons in the CB of $SrTiO_3$ will migrate to the MoS_2, which makes the electrons more mobile and provides highly active sites for the photocatalysis process. In addition, the holes left in the $SrTiO_3$ can be consumed by the MO dyes. The above mentioned way in which photo-generated electrons in the CB of $SrTiO_3$ are transferred improves the separation of the photo-generated electron−hole pairs, effectively suppressing recombination between electrons and holes, enhancing interfacial charge transfer, lengthening the lifetime of the charge carriers and enlarging the active sites. Consequently, the $MoS_2/SrTiO_3$ composites can retard the photogenerated electron-hole pairs recombination and prolong the lifetime of the electron-hole pairs, enhancing the photocatalytic activity for degradation of MO organic dyes.

4 Conclusions

In summary, in this study, the simple two-step hydrothermal synthesis of $MoS_2/SrTiO_3$ composite materials afforded an effective photocatalyst for degradation of MO organic dyes under UV light irradiation. The $MoS_2/SrTiO_3$ composite photocatalyst showed excellent photocatalytic degradation rate with a rate of 99.81% in 60 min for the optimal sample consisting of 99.95 wt % $SrTiO_3$ and 0.05 wt % MoS_2, which is dramatically higher than that of pure $SrTiO_3$. In addition, a suitable loading content of MoS_2 is crucial for optimizing the photocatalytic performance of $MoS_2/SrTiO_3$ composites. This is due to the fact that excessive loading of MoS_2 can shield the active sites and also decrease the intensity of UV light irradiation. The possible photocatalytic mechanism is also proposed. It is believed that the effect of loading MoS_2 can efficiently suppress electron-hole pairs recombination and improve interfacial charge transfer, leading to the photocatalytic degradation activity. This study demonstrates that the development of cheap non-noble-metal and environmentally benign semiconductor-based composites such as $MoS_2/SrTiO_3$ is feasible and this high efficiency photocatalyst has a great potential for degradation of organic dyes.

Notes and references

School of Chemistry and Chemical Engineering, Southeast University, Nanjing, 211189, P.R. China.
Fax: +86 02552090620; Tel: +86 025 52090621; E-mail: jczhou@seu.edu.cn (Prof. J. Zhou)
† These authors contributed equally to this work.

1 F. Han, V.S.R. Kambala, M. Srinivasan, D. Rajarathnam and R. Naidu, *Applied Catalysis A: General*, 2009, **359**, 25.
2 B. L. Fei, W. Li, J. H. Wang, Q. B. Liu, J. Y. Long, Y. G. Li, K. Z. Shao, Z. M. Su and W. Y. Sun, *Dalton Transaction*, 2014, **43**, 10005.
3 J. Z. Yang, J. W. Yu, J. Fan, D. P. Sun, W. H. Tang and X. J. Yang, *Journal of Hazardous materials*, 2011, **189**, 377.
4 Z. Yu, F. Y. Qu and X. Wu, *Dalton Transaction*, 2014, **43**, 4847.
5 C.A. Martínez-Huitle, E. Brillas, *Applied Catalysis B: Environmental*, 2009, **87**, 105.
6 V. Polshettiwar, R. Luque, A. Fihri, H. B. Zhu, M. Bouhrara and J. M. Basset, *Chemical Reviews*, 2011, **111**, 3036.
7 F. Fresno, R. Portela, S. Suárez and J. M. Coronado, *Journal of Materials Chemistry A*, 2014, **2**, 2863.
8 C. Li, J. Wang, S. Feng, Z. Yang and S. Ding, *Journal of Materials Chemistry A*, 2013, **1**, 8045.
9 M. Basu, N. Garg and A. K. Ganguli, *Journal of Materials Chemistry A*, 2014, **2**, 7517.
10 M. Mecklenburg, A. Schuchardt, Y. K. Mishra, S. Kaps, R. Adelung, A. Lotnyk, L. Kienle and K. Schulte, *Advanced Materials*, 2012, **24**, 3486.
11 H. Bai, Z. Liu, L. Liu and D. D. Sun, *Chemistry-A European Journal*, 2013, **19**, 3061.
12 Y. Min, G. He, Q. Xu and Y. Chen, *Journal of Materials Chemistry A*, 2014, **2**, 2578-2584.
13 S. Kumar, T. Surendar, A. Baruah and V. Shanker, *Journal of Materials Chemistry A*, 2013,**1**, 5333.
14 F. Bai, Z. Sun, H. Wu, R. E. Haddad, E. N. Coker, J. Y. Huang, M. A. Rodriguez and H. Fan, *Nano Letters*, 2011, **11**, 3759.
15 F. Bai, Z. Sun, H. Wu, R. E. Haddad, X. Xiao, and H. Fan, *Nano Letters*, 2011, **11**, 5196.
16 Y. Zhong, Z. Wang, R. Zhang, F. Bai, H. Wu, R. Haddad and H. Fan, *ACS NANO*, 2014, **1**, 827.
17 P. Xiao, H. L. Li, T. Wang, X. L. Xu, J. L. Lia and J. J. Zhu, *RSC Advances*, 2014, **24**, 12601.
18 M. A. Pena and J. L. G. Fierro, *Chemical Reviews*, 2001, **7**, 1981.
19 T. Ohnoa, T. Tsubotaa, Y. Nakamuraa and K. Sayama, *Applied Catalysis A: General*, 2005, **1-2**, 74.
20 H. Tong, S. X. OuYang, Y. P. Bi, N. Umezawa, M. Oshikiri and J. H. Ye, *Advanced Materials*, 2012, **2**, 229.
21 U. I. Gaya and A. H. Abdullah, *Journal of Photochemistry and Photobiology C: Photochemistry Reviews*, 2008, **1**, 1.
22 A. Kudo and Y. Miseki, *Chemical Society Reviews*, 2009, **1**, 253.
23 K. Iwashina and A. Kudo, *Journal of the American Chemical Society*, 2011, **34**, 13272.
24 P. Khunrattanaphon, S. Chavadej and T. Sreethawong, *Chemical Engineering Journal*, 2011, **1**, 292.
25 G. C. Xi, B. Yue, J. Y. Cao and J. H. Ye, *Chemistry-A European Journal*, 2011, **18**, 5145.

26 J. Lv, T. Kako, Z. S. Li, Z. G. Zou and J. H. Ye, *Journal of Physical Chemistry C*, 2010, **13**, 6157.

27 T. Kako and J. H. Ye, *Journal of Molecular Catalysis A: Chemical*, 2010, **1-2**, 79.

28 W. J. Zhou, Z. Y. Yin, Y. P. Du, X. Huang, Z. Y. Zeng, Z. X. Fan, H. Liu, J. Y. Wang and H. Zhang, *Small*, 2013, **1**, 140.

29 G. P. Chen, D. M. Li, F. Li, Y. Z. Fan, H. F. Zhao, Y. H. Luo, R. C. Yu and Q. B. Meng, *Applied Catalysis A: General*, 2012, **443-444**, 138.

30 Y. L. Min, G. Q. He, Q. J. Xu and Y. C. Chen, *Journal of Materials Chemistry A*, 2014, **8**, 2578.

31 L. Ge, C. C. Han, X. L. Xiao and L. L. Guo, *International Journal of Hydrogen Energy*, 2013, 1**7**, 6960.

32 J. L. Li, X. J. Liu, L. K. Pan, W. Qin, T. Q. Chen and Z. Sun, *RSC Advances*, 2014, **4**, 9647.

33 Q. J. Xiang, J. G. Yu and M. Jaroniec, *Journal of the American Chemical Society*, 2012, **15**, 6575.

34 L. Wei, Y. J. Chen, Y. P. Lin, H. S. Wu, R. S. Yuan and Z. H. Li, *Applied Catalysis B: Environmental*, 2014, **144**, 521.

35 X. Zong, J. F. Han, G. J. Ma, H. J. Yan, G. P. Wu and C. Li, *Journal of Physical Chemistry C*, 2011, **24**, 12202.

36 W. H. Kim and J. Y. Son, *Bulletin of the Korean Chemical Society*, 2013, **9**, 2563.

37 B. K. Bubmann, K. Marinov, O. Ochedowski, N. Scheuschner, J. Maultzsch and M. Schleberger, *MRS Online Proceedings*, 2012, 1474.

38 S. X. Ouyang, H. Tong, N. Umezawa, J. Y. Cao, P. Li, Y. P. Bi, Y. J. Zhang and J. H. Ye, *Journal of the American Chemical Society*, 2012, **4**, 1974.

39 L. F. Silva, J. C. M'Peko, J. Andrés, A. Beltrán, L. Gracia, M. I. B. Bernardi, A. Mesquita, E. Antonelli, M. L. Moreira and V. R. Mastelaro, *Journal of Physical Chemistry C*, 2014, **118**, 4930.

40 J. W. Ng, S. P. Xu, X. W. Zhang, H. Y. Yang and D. D. Sun, *Advanced Functional Materials*, 2010, **20**, 4287.

41 W. K. Ho, J. C. Yu, J. Lin, J. G. Yu and P. S. Li, *Langmuir*, 2004, **14**, 5865.

42 C. Karunakaran, S. SakthiRaadha, P. Gomathisankar and Pazhamalai Vinaya, *Dalton transactions*, 2013, **42**, 13855

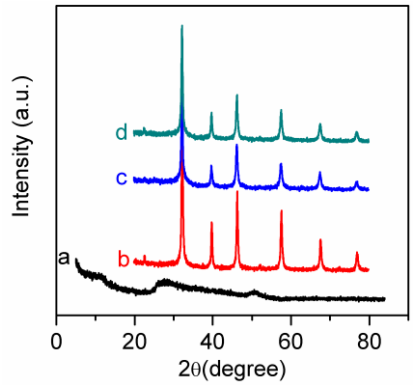

Fig. 1 XRD patterns of (a) pure MoS_2, (b) pure $SrTiO_3$, (c) 0.05 wt % $MoS_2/SrTiO_3$ and (d) 5.0 wt % MoS_2/ $SrTiO_3$ composites.

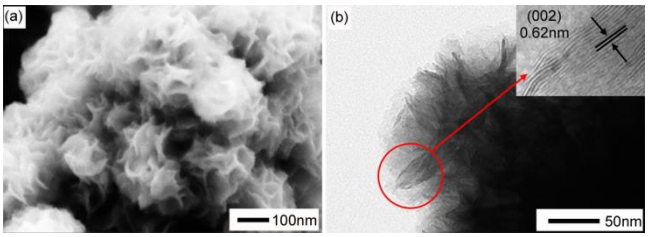

Fig. 2 (a) SEM images of pure MoS_2, and (b) TEM images of pure MoS_2.

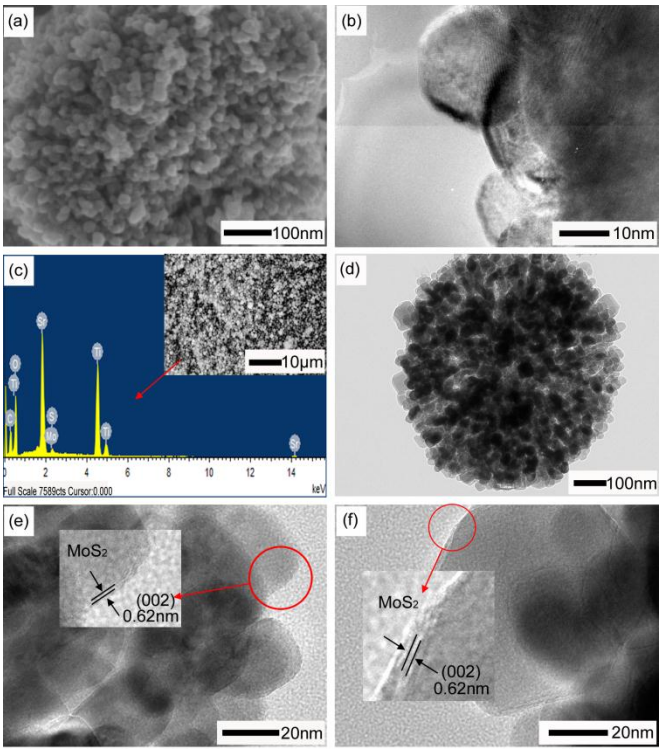

Fig. 3 (a) SEM images of $SrTiO_3$, (b) TEM images of $SrTiO_3$, (c) EDS of 5 wt % MoS_2/ $SrTiO_3$ and (d), (e), (f) TEM images of 5 wt % $MoS_2/SrTiO_3$,

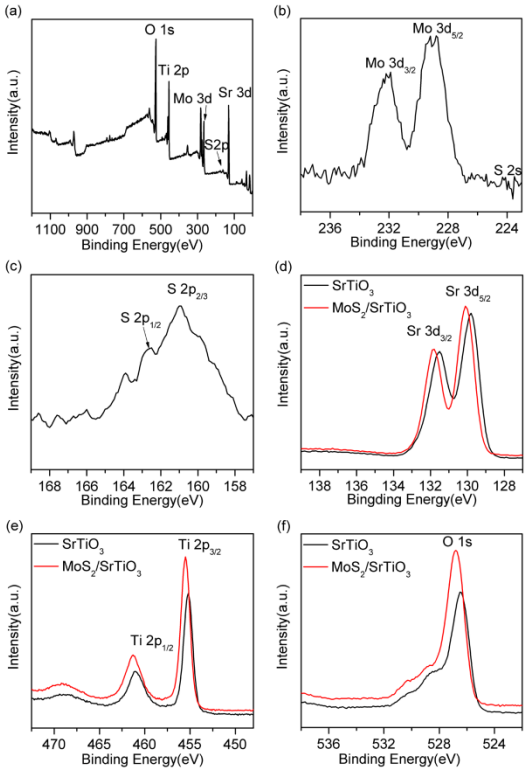

Fig. 4 XPS spectra of (a) 5 wt % $MoS_2/SrTiO_3$, XPS spectra of (b) Mo 3d, (c) S 2p, (d) Sr 3d, (e) Ti 2p, and (f) O 1s peaks.

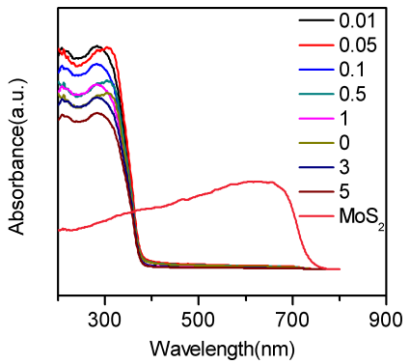

Fig. 5 UV-Vis diffuse reflectance spectra of pure MoS_2, pure $SrTiO_3$, and $MoS_2/SrTiO_3$ composites.

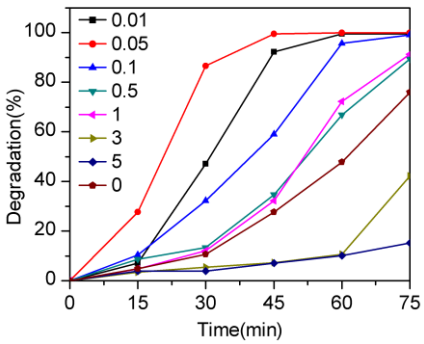

Fig. 6 The degradation performance of pure $SrTiO_3$ and $MoS_2/SrTiO_3$ composites in 90 min.

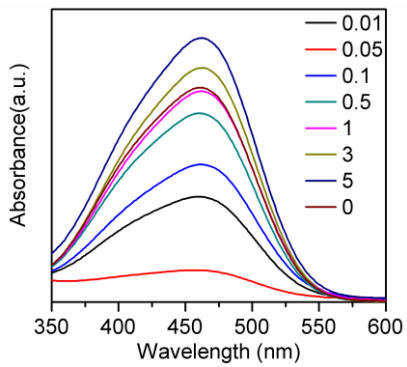

Fig. 7 UV-vis absorption of MO with the variation of MoS_2 loading at 30 min irradiation time.

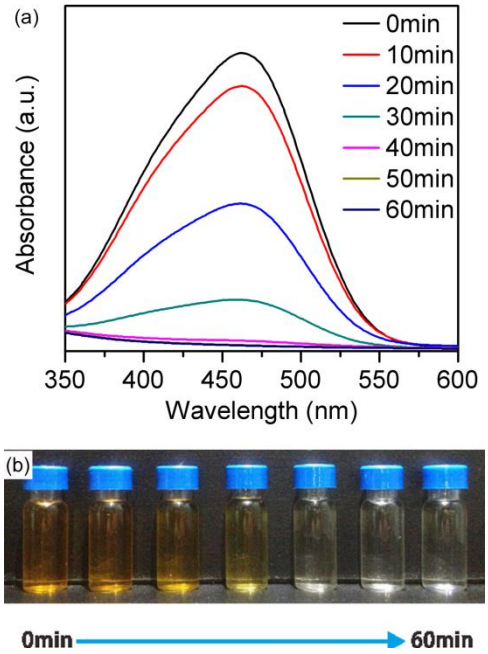

Fig. 8 (a)UV-vis absorption of MO with the variation of irradiation time using 0.05 wt % $MoS_2/SrTiO_3$ composites, and (b) The colour of MO dyes solutions changes with the variation of irradiation time using 0.05 wt % $MoS_2/SrTiO_3$ composites.

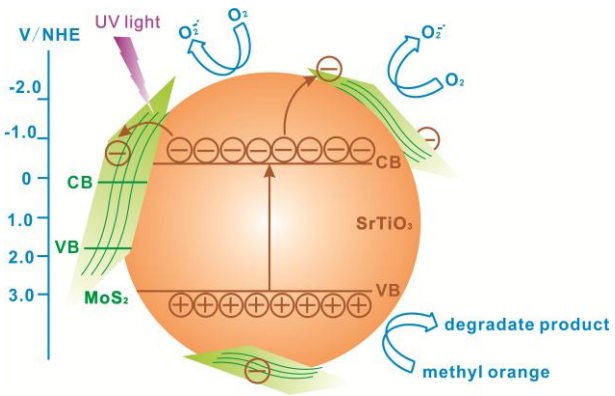

Fig. 9 The proposed mechanism of the charge transfer and separation process for the $MoS_2/SrTiO_3$ composites under UV irradiation.

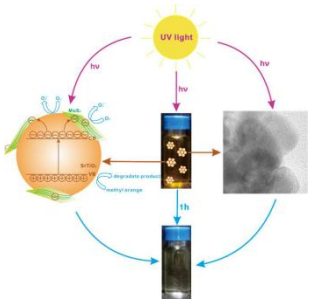

A novel composite material $MoS_2/SrTiO_3$ can show the excellent photocatalytic activity with the degradation rate as high as 99.81%.